Pliocene–Pleistocene incision of the Green River, Kentucky, determined from radioactive decay of cosmogenic ^{26}Al and ^{10}Be in Mammoth Cave sediments

Darryl E. Granger*
Derek Fabel†
Purdue Rare Isotope Measurement Laboratory, Department of Earth and Atmospheric Sciences, Purdue University, West Lafayette, Indiana 47907-1397, USA

Arthur N. Palmer
Department of Earth Sciences, State University of New York, College at Oneonta, Oneonta, New York 13820-4015, USA

ABSTRACT

Cosmogenic ^{26}Al and ^{10}Be in sediments washed into Mammoth Cave, Kentucky, record the history of 3.5 m.y. of water-table position, governed by incision and aggradation of the Green River, a tributary of the Ohio River. Upper levels of the cave formed during a period of slow river incision and were later filled with sediment due to river aggradation at 2.3–2.4 Ma. A brief surge of river incision ca. 2 Ma was followed by river stability and cave-passage formation at a lower level. Rapid incision through 15 m of bedrock ca. 1.5 Ma was prompted by repositioning of the Ohio River to its present course along an ice-sheet margin. Renewed incision ca. 1.2 Ma and aggradation at 0.7–0.8 Ma correlate with major ice advances in the Ohio River basin. Measurements of ^{26}Al and ^{10}Be also indicate that sandstone-capped uplands have maintained slow erosion rates of 2–7 m/m.y. for the past 3.5 m.y., despite accelerated Pleistocene river incision rates of ~30 m/m.y.

Keywords: cosmogenic elements, geochronology, karst, landscape evolution, Mammoth Cave, Ohio River basin.

INTRODUCTION

Landscape development in the Interior Low Plateaus region of the east-central United States has been profoundly influenced by Pliocene–Pleistocene glaciation (Thornbury, 1965; Teller and Goldthwait, 1991). Although the region is entirely south of the Laurentide ice-sheet margin, north-flowing rivers have been repeatedly dammed and diverted by ice sheets (Fig. 1). Alternating river incision and sedimentation along the ice margins have promoted regional river entrenchment and episodic aggradation to the south (e.g., Melhorn and Kempton, 1991).

The region is characterized by low cuestas developed on erosion-resistant strata around the perimeter of the Illinois basin and Nashville dome (Fenneman, 1938). One of the most prominent cuestas is the Chester upland, which is capped by Upper Mississippian and Lower Pennsylvanian sandstone and conglomerate, and forms an escarpment overlooking broad plains developed on underlying Mississippian limestones. The limestone extends across much of the Interior Low Plateaus, forming the largest expanse of cavernous rock in North America (Davies and LeGrand, 1972).

Mammoth Cave, Kentucky, the longest known cave in the world, is located at the southeastern edge of the Chester upland. It contains 560 km of mapped interconnected passages that span a vertical range of ~200 m. Its passages were formed by the dissolution of limestone by groundwater in the form of discrete underground streams, fed by surface runoff entering sinkholes, in combination with diffuse infiltration. As surface rivers entrench their valleys, cave passages form at progressively lower elevations at and just below the water table (e.g., White, 1998; Ford and Williams, 1987). Aggradation of surface rivers floods the lowest cave passages, allowing many to be filled with clastic sediment carried by underground streams. Thus, the development of this kind of cave is closely controlled by the local history of fluvial entrenchment and aggradation (Bocchini and Coltorti, 1990; Davies, 1960; Powell, 1970; White, 1988, p. 264–301).

Rivers in the Interior Low Plateaus join the Ohio River and are almost all deeply entrenched (Fenneman, 1938). Entrenchment occurred in at least two stages, as inferred from broad straths in the plateau surfaces that have narrower canyons cut into them (Teller and Goldthwait, 1991; see Thornbury, 1965, for discussion). Tight (1903) recognized that the most recent episode of regional river entrenchment was triggered by rapid incision of the Ohio River soon after it acquired its present course along an ice-sheet margin (for reviews see Ray, 1974; Melhorn and Kempton, 1991). The onset of river entrenchment has been ascribed to both epeirogenic uplift (Potter, 1955) and climate change (e.g., Teller and Goldthwait, 1991). However, the uncertain chronology of river incision and strath formation has precluded a firm correlation of river incision with the climate record (Ray, 1974).

Our goal is to clarify the fluvial chronology in the Interior Low Plateaus by dating quartzose sediments at the various levels in Mammoth Cave using cosmogenic ^{26}Al and ^{10}Be and relating the evolution of the cave to that of the regional drainage pattern. To achieve this goal, it is essential to confirm the relation between cave passages and local fluvial base level.

*E-mail: dgranger@purdue.edu.
†Present address: School of Earth Sciences, University of Melbourne, Victoria 3010, Australia.

GSA Bulletin; July 2001; v. 113; no. 7; p. 825–836; 5 figures; 4 tables.

Mammoth Cave and its Relation to Surface Rivers

The development of Mammoth Cave has been controlled by the erosional-depositional history of the Green River. Nearly all groundwater in the cave area emerges through springs at the river level, which dictates the local water-table elevation. The water table has very low relief because of the high permeability of the cavernous limestone. The cave is mainly in the updip portions of the Chester upland (Fig. 2), although its largest tributaries are fed by sinking streams and dolines in the sinkhole plain to the southeast.

Cave passages form along the paths of greatest groundwater discharge through soluble rock (Palmer, 1991; Dreybrodt, 1996). In the prominently bedded strata of the Mammoth Cave region, those passages formed above the water table consist of narrow, sinuous, and entrenched canyon-like conduits oriented almost invariably down the local dip of the strata, and are interspersed with vertical shafts discordant to the bedding. Passages formed below the water table are mainly tubular conduits that have no consistent relation to the dip. Most passages contain an upstream vadose section formed above the water table and a contemporaneous downstream phreatic section formed below the water table (Palmer, 1991). If the water table remained fairly stable throughout the evolution of the phreatic segment, then the vadose-phreatic transition can be clearly recognized by the change in passage shape and loss of dip orientation, both of which mark the position of the former water table. These vadose-phreatic transitions remain clearly preserved, even in passages that are now dry, and provide a record of water-table lowering.

As fluvial entrenchment lowers the local water table, former phreatic passages become air filled. Passages at the highest elevations are oldest, as can be verified by crosscutting relationships at passage intersections, paleomagnetic sediment dating (Schmidt, 1982), and our $^{26}Al/^{10}Be$ sediment dating. This type of cave can be used to determine river history in a manner analogous to river terraces. Periods of river stability are represented on the surface by wide straths cut into bedrock, whereas they are represented underground by large cave passages with distinct vadose-phreatic transitions occurring at the same elevation over a broad region. Rapid river incision is represented on the surface by narrow canyons, whereas in caves, rapid incision causes phreatic tubes to be abandoned in favor of narrow vadose canyons. River aggradation is represented on the surface by alluvial terraces and underground by sediment-filled caves.

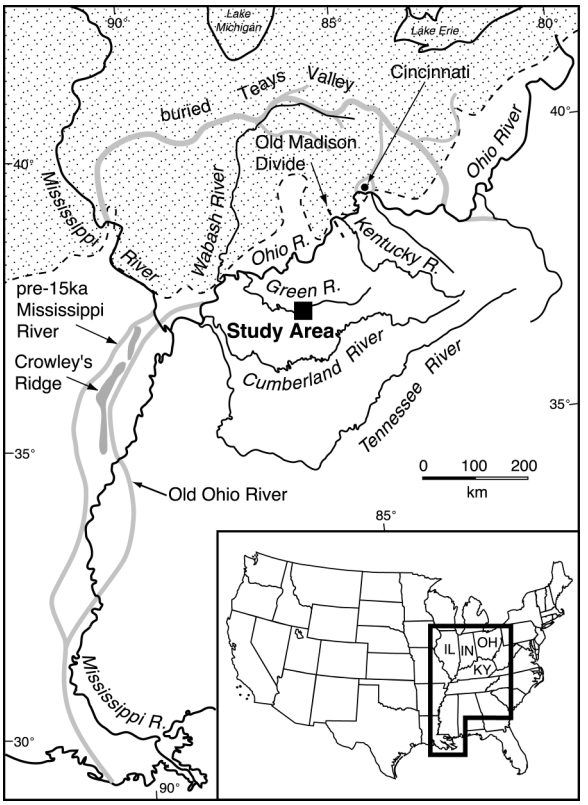

Figure 1. Map showing study area with respect to major ancient and modern rivers. Note that the preglacial Old Ohio River headed at Madison, Indiana, and that Crowley's Ridge separated the Ohio and Mississippi Rivers until the last glacial maximum (Royall et al., 1991). Stippled area denotes approximate maximum glacial extent. The Interior Low Plateaus province stretches roughly from the Tennessee River to the glacial boundary (after Thornbury, 1965; Teller and Goldthwait, 1991; Fisk, 1944).

The Mammoth Cave system contains vadose-phreatic transitions at several distinct elevations (Table 1). Geologic surveys of the major passages were made with an automatic tripod-mounted level (or hand level in small passages) in order to quantify passage gradients, structural relationships, and the elevations of vadose-phreatic transitions throughout the cave system (Palmer, 1977, 1989). These surveys show a consistent vertical zonation of passage types. Relict vadose-phreatic transition zones are easily recognized at several distinct altitudes, deviating <2 m among the passages within any given group. These distinct levels are independent of stratigraphy because different passages at the same level occupy different strata.

The uppermost (oldest) passages were graded to the river level at the present elevation of 175–215 m. They are designated levels A and B (Palmer, 1981) and include wide canyons and tubes containing thick stream deposits of quartzose sand and gravel. The most prominent vadose-phreatic transition is at the present elevation of 189 m. These passages are interpreted to be the result of slow fluvial entrenchment in late Tertiary time, interrupted periodically by significant aggradation (Miotke and Palmer, 1972).

In underlying passages the major vadose-phreatic transitions are concentrated at altitudes of 166–168 m and 151–152 m (levels C and D of Palmer, 1981). The major passages are phreatic tubes containing little sediment fill. These levels were interpreted by Miotke and Palmer (1972) to represent rapid Quaternary base-level fluctuations.

Most of the Mammoth Cave system is overlain by sandstone, which is the source for abundant sand deposits and rounded sandstone cobbles in the cave. Basal Pennsylvanian conglomerate, now surviving only as remnants on ridge crests, supplies rounded quartz pebbles to the cave. Most of the clastic sediment enters the headwater regions of the cave through sinking streams and subsidence of colluvium

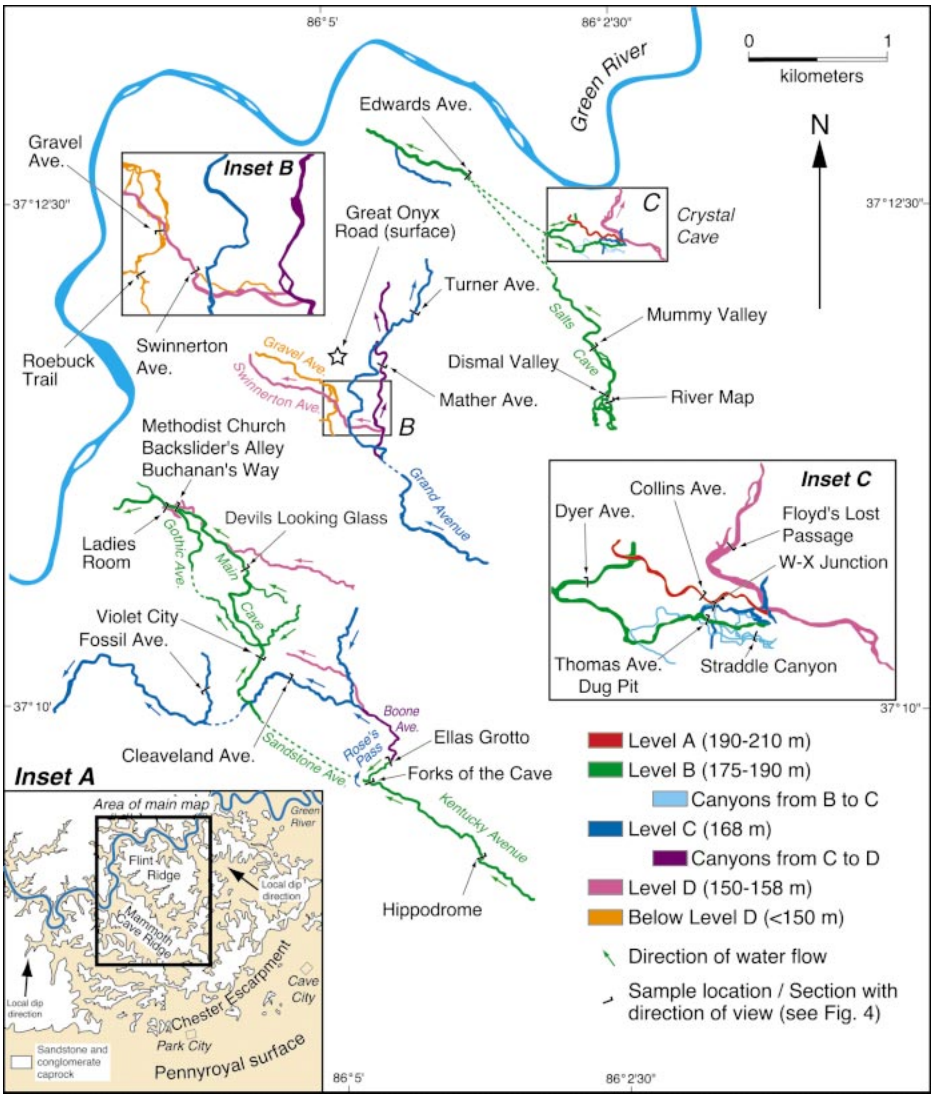

Figure 2. Partial map of the Mammoth Cave system, showing important passage relationships. Sampled sites are labeled; descriptions are in Table 3, and cross sections are shown in Figure 3. Caves are developed in limestone beneath sandstone- and conglomerate-capped ridges of the Chester upland (inset A). Limestones crop out on the Pennyroyal surface (inset A) and drain to the Green River via the Mammoth Cave system. Cave levels and intermediate passages are separated by color. Dashed lines indicate probable conduits that have been destroyed by upland dissection and cave collapse. Insets B and C provide detail of passage relationships.

TABLE 1. PERSISTENT VADOSE-PHREATIC TRANSITIONS IN THE MAMMOTH CAVE SYSTEM

Level	Elevation (m)	Typical characteristics	Associated local surface features and events
A	~200	Large passages once filled with sediment	Caprock breached by Green River
B	170–180	Very large passages (>100 m²) once filled with sediment	Broad straths mantled with 6–10 m alluvium Karst plain development (Pennyroyal surface) Karst valley floors graded to this level
C	167	Large passages (~30 m²) with sparse sediment	Strath in Green River gorge
D	150	Small passages (~10 m²) with sparse sediment	Strath in Green River gorge
Lower	Complex	Small passages with no regional vadose-phreatic transition	Wisconsinan-age alluvial sediment in Green River

in sinkholes. Finer grained sediment is deposited by backflooding from the Green River (White and White, 1968). Coarse sediment carried by cave streams is deposited contemporaneously with active passage enlargement and is thus a valid indication of the contemporary altitude of the Green River, although fine-grained silts and clays can be deposited by floods reaching 20 m or more above base level.

Because the sand and gravel deposits in the cave represent the last stages of passage growth, they can reveal the erosional and depositional history of the Green River since late Tertiary time. We use ^{26}Al and ^{10}Be to date quartz sediments preserved in many of the cave trunk passages in order to determine the timing of river incision, stability, and aggradation over the past ~3.5 m.y.

BURIAL DATING WITH COSMOGENIC ^{26}Al AND ^{10}Be

The cosmogenic radionuclides ^{26}Al and ^{10}Be are produced in quartz near the ground surface by reactions with secondary cosmic ray neutrons and muons (Lal and Peters, 1967). Neutron cascades generated in the atmosphere penetrate rocks at the Earth's surface, producing ^{26}Al and ^{10}Be by spallation of ^{28}Si and ^{16}O nuclei. Muons produced in the upper atmosphere likewise generate ^{26}Al and ^{10}Be as they are slowed and captured by nuclei within the quartz (Rossi, 1948; Lal and Peters, 1967; Bilokon et al., 1989). Neutron spallation accounts for ~98% of ^{26}Al and ^{10}Be production at the surface, and muons account for the remaining ~2% (Heisinger, 1998). Although neutrons dominate cosmogenic nuclide production at the surface, they are more rapidly attenuated than muons, which dominate at depth. The neutron flux decreases exponentially with a penetration length of 160 ± 10 g cm^{-2}, or 57 cm in rock of density 2.8 g cm^{-3} (Masarik and Reedy, 1995), whereas the muon stopping rate declines to 1/*e* of its surface value at ~1000 g cm^{-2}, and 1/*e*^{2} of its surface value at ~2200 g cm^{-2} (see Stone et al., 1998). Fast muon reactions decrease with an *e*-folding length of 4360 g cm^{-2} near the surface (Heisinger, 1998; Granger and Smith, 2000).

Because cosmogenic radionuclides are produced only near the ground surface, they can be used to date sediments that were once exposed to cosmic radiation and were subsequently buried. Burial dates are inferred from the relative radioactive decay of ^{26}Al and ^{10}Be in buried sediments. Because ^{26}Al decays more rapidly than ^{10}Be, the ^{26}Al/^{10}Be ratio decreases exponentially with burial time (radio-

active mean lives are $\tau_{26} = 1.02 \pm 0.06$ Ma [Norris et al., 1983], and $\tau_{10} = 2.18 \pm 0.09$ Ma [Hofmann et al., 1987]). Preburial concentrations of ^{26}Al and ^{10}Be can be inferred from simple models of cosmogenic nuclide accumulation at the surface.

In most soil-mantled landscapes, bedrock is gradually weathered, decomposed into regolith, and carried downslope. Cosmogenic radionuclide accumulation in the regolith may be modeled for the simple case of steady-state erosion (Lal and Arnold, 1985; Lal, 1991). A quartz grain within eroding bedrock is exposed to increasingly intense cosmic radiation over time as it approaches the ground surface and is eventually carried downslope. While ^{26}Al and ^{10}Be accumulation in quartz grains can be complicated in detail, depending upon the density changes from bedrock to soil (Brown et al., 1994) and vertical mixing within the regolith, a simple steady-state erosion model provides a good approximation for cosmogenic nuclide concentrations in the regolith (Brown et al., 1995; Bierman and Steig, 1996; Granger et al., 1996). In this case, the concentration (N_i) of either ^{26}Al or ^{10}Be in quartz at the surface can be determined from equation 1:

$$N_i = P_n/(1/\tau_i + \rho E/\Lambda_n) + P_\mu/(1/\tau_i + \rho E/\Lambda_\mu), \quad (1)$$

where P_n is production rate by neutrons, P_μ is production rate by muons, ρ is density, E is erosion rate, and Λ_n and Λ_μ are penetration lengths for neutrons and muons (we use $\Lambda_\mu = 1300$ g cm^{-2} from Brown et al., 1995; equation 1 is modified from Lal, 1991). Equation 1 assumes that the muon stopping rate decreases exponentially with depth, which is a sufficient approximation for these calculations. A more accurate accounting of muogenic production can be made (Stone et al., 1998; Heisinger, 1998; Granger and Smith, 2000), but is beyond the needs of this paper.

In some special cases, ^{26}Al and ^{10}Be accumulation in sediments may be more accurately modeled as if the quartz grains were instantaneously exposed at the surface (e.g., in sediments derived from a landslide scar [Kubik et al., 1998] or a glacially scoured valley [e.g., Nishiizumi et al., 1989]). In these cases, the radionuclide concentrations are given by equation 2,

$$N_i = (P_{n,i} + P_{\mu,i})\,\tau_i\,[1 - e^{-t/\tau_i}]. \quad (2)$$

where t is exposure time. Quartz sediment at the ground surface should have cosmogenic nuclide concentrations determined by equations 1 or 2. If the sediment is suddenly shielded from cosmic radiation (e.g., by being washed into a cave, deposited in a lake, or buried beneath deep alluvial sediments), then ^{26}Al and ^{10}Be production drastically slows or ceases. Radioactive decay then lowers the inherited ^{26}Al/^{10}Be ratio over time (Lal and Arnold, 1985; Klein et al., 1986), according to equation 3:

$$N_{26}/N_{10} = [N_{26}/N_{10}]_0\, e^{-t(1/\tau_{26} - 1/\tau_{10})}, \quad (3)$$

where $[N_{26}/N_{10}]_0$ represents the inherited ^{26}Al/^{10}Be ratio as determined from equations 1 or 2. Because ^{26}Al and ^{10}Be concentrations in buried sediment depend on two unknowns (burial time and preburial concentrations), equation 3 must be coupled with either equation 1 or 2 to solve for both burial time and either the preburial erosion rate or exposure time.

The models used to infer preburial cosmogenic nuclide concentrations include assumptions that must be understood for uncertainty analysis. Both equations 1 and 2 assume uniform production rates through time; variations in production rates arise due to geomagnetic field strength fluctuation (e.g., Frank et al., 1997). However, because production rate variations affect ^{26}Al and ^{10}Be alike, they have very little effect on the initial ^{26}Al/^{10}Be ratio. Production rate variations therefore have little effect on burial dating, but may have a strong effect on estimates of preburial erosion rates.

Equation 1 assumes steady-state bedrock erosion. Dramatic erosion rate variations can potentially lower ^{26}Al/^{10}Be ratios in sediment, but only if erosion rates are sufficiently slow ($<<10$ m/m.y.) that sediment spends hundreds of thousands of years within the zone of rapid cosmogenic nuclide production near the surface. More commonly, the inherited ^{26}Al/^{10}Be ratio can be lowered by periodic sediment burial, for example within accumulating soils (Brown et al., 1994), within alluvial terraces (Granger et al., 1997), within migrating sand dunes (Middleton and Klein, 1987), or beneath ice cover (Bierman et al., 1999; Fabel and Harbor, 1999).

Significant lowering of the ^{26}Al/^{10}Be ratio requires sediment burial over time scales comparable to ^{26}Al decay ($\tau = 1.02$ m.y.). Despite these limitations in certain environments, the ^{26}Al/^{10}Be ratio in most soil-mantled landscapes should fall very near the steady-state erosion approximation of equation 1. Our data from this study at the Mammoth Cave area confirm the steady-state erosion approximation at this site (Table 2; Fig. 4). Moreover, many erosion-rate studies have demonstrated that surface sediments conform to the expected ^{26}Al/^{10}Be ratio near 6.0 (Granger et al., 1996; Heimsath et al., 1997; Brown et al., 1995; Repka et al., 1997; Small et al., 1999). Nonetheless, burial dates should be strictly considered as maximum ages, with the caveat that sediments could have conceivably undergone an earlier burial episode.

METHODS

Sample Collection

We collected quartz gravel and sand from 29 sedimentary deposits throughout the Mammoth Cave system and from the surface (Table 3). Because interpretation of the sediment's depositional environment is crucial for reconstructing the cave's evolution and the water-table history, we focused most of our sampling effort on large phreatic tubes and vadose canyons with clear geomorphic relationships to the history of the Green River. Sample locations within the cave system are shown in Figure 2, and cave-passage cross sections and elevations are shown to scale in Figure 3. Descriptions of sampling locations and their geomorphic relationships are included as Table 3. Sample elevations were determined from either leveling surveys or a surveying altimeter and are accurate to within 1–2 m.

Gravel samples were derived from the overlying Caseyville conglomerate and were washed into the cave as the bedload of sinking streams. Sand samples, however, were derived from the Big Clifty and Hardinsburg Formations. The Big Clifty directly overlies the cave-forming limestones, so some of the sand could have entered the cave through doline collapse. However, the limited number of doline collapse features in the cave suggests that most of the sand was brought into the cave by sinking streams. Wherever possible, we collected Caseyville gravels because their deposition as bedload closely marks the level of underground rivers. Sand samples may be more difficult to interpret because they can be deposited by floodwaters that reach far above the prevailing water table, and they may be more easily remobilized from upper levels of the cave.

Cosmogenic Nuclide Chemistry

Gravel samples were handpicked for clear, white quartz and typically included 50–100 clasts. Sand samples were sieved to 0.25–0.5 mm, the modal grain size of the Big Clifty sandstone, to exclude occasional chert clasts

TABLE 2. COSMOGENIC NUCLIDE DATA, EROSION RATES, AND BURIAL AGES

Sample	Sample type	[^{26}Al]* (10^6 at g^{-1})	[^{10}Be]* (10^6 at g^{-1})	[^{26}Al]/[^{10}Be]	Erosion rate† (m m.y.$^{-1}$)	Burial age† (Ma)
Great Onyx Road	Gravel	8.719 ± 0.567	1.680 ± 0.024	5.19 ± 0.23	1.72 ± 0.07 (0.39)	−0.02 ± 0.07 (0.13)
Roebuck Trail	Gravel	0.276 ± 0.017	0.732 ± 0.018	3.76 ± 0.17	3.08 ± 0.13 (0.69)	0.70 ± 0.08 (0.15)
Gravel Avenue	Gravel	2.320 ± 0.178	0.937 ± 0.023	2.48 ± 0.16	1.60 ± 0.10 (0.40)	1.38 ± 0.10 (0.19)
Floyd's Lost Passage	Gravel	1.451 ± 0.093	0.520 ± 0.022	2.79 ± 0.16	3.35 ± 0.18 (0.78)	1.28 ± 0.10 (0.18)
Buchanan's Way	Gravel	1.894 ± 0.106	0.518 ± 0.023	3.66 ± 0.18	4.31 ± 0.20 (0.96)	0.80 ± 0.09 (0.16)
Ladies Room	Gravel	1.410 ± 0.100	0.522 ± 0.010	2.70 ± 0.15	3.25 ± 0.16 (0.76)	1.34 ± 0.09 (0.18)
Swinnerton Avenue	Gravel	1.964 ± 0.129	0.703 ± 0.019	2.79 ± 0.14	2.44 ± 0.12 (0.58)	1.23 ± 0.09 (0.17)
Mather Avenue	Gravel	2.203 ± 0.160	0.787 ± 0.034	2.80 ± 0.19	2.17 ± 0.14 (0.52)	1.21 ± 0.12 (0.19)
W-X Junction	Gravel	1.975 ± 0.130	0.662 ± 0.021	2.99 ± 0.16	2.77 ± 0.14 (0.65)	1.13 ± 0.09 (0.17)
Cleaveland Avenue	Gravel	0.854 ± 0.051	0.303 ± 0.025	2.82 ± 0.25	5.91 ± 0.47 (1.40)	1.34 ± 0.15 (0.22)
Turner Avenue	Gravel	1.190 ± 0.074	0.466 ± 0.018	2.56 ± 0.14	3.47 ± 0.17 (0.82)	1.46 ± 0.09 (0.19)
Fossil Avenue	Gravel	1.453 ± 0.102	0.498 ± 0.009	2.92 ± 0.15	3.65 ± 0.18 (0.84)	1.21 ± 0.09 (0.18)
Edwards Avenue	Gravel	1.340 ± 0.089	0.544 ± 0.010	2.46 ± 0.12	2.85 ± 0.12 (0.68)	1.50 ± 0.08 (0.19)
Methodist Church	Sand	0.281 ± 0.046	0.197 ± 0.084	1.43 ± 0.23	4.97 ± 0.73 (1.45)	2.62 ± 0.27 (0.36)
Devil's Looking Glass	Gravel	1.426 ± 0.096	0.571 ± 0.015	2.50 ± 0.13	2.74 ± 0.13 (0.65)	1.47 ± 0.09 (0.19)
Forks of the Cave	Sand	0.669 ± 0.066	0.303 ± 0.016	2.21 ± 0.22	4.75 ± 0.43 (1.19)	1.78 ± 0.17 (0.25)
Straddle Canyon	Gravel	0.782 ± 0.058	0.398 ± 0.009	1.96 ± 0.12	3.21 ± 0.17 (0.80)	1.95 ± 0.10 (0.22)
Violet City	Gravel	0.719 ± 0.060	0.442 ± 0.018	1.63 ± 0.13	2.42 ± 0.18 (0.64)	2.27 ± 0.13 (0.25)
Dug Pit Sand	Sand	0.268 ± 0.045	0.190 ± 0.009	1.41 ± 0.24	5.12 ± 0.77 (1.51)	2.65 ± 0.28 (0.37)
Dug Pit Gravels	Gravel	0.636 ± 0.040	0.368 ± 0.018	1.73 ± 0.11	3.10 ± 0.18 (0.79)	2.19 ± 0.11 (0.24)
River Map	Gravel	0.842 ± 0.052	0.444 ± 0.023	1.90 ± 0.12	2.77 ± 0.16 (0.70)	2.00 ± 0.11 (0.22)
Mummy Valley	Gravel	1.421 ± 0.101	0.580 ± 0.011	2.45 ± 0.13	2.65 ± 0.13 (0.64)	1.50 ± 0.09 (0.19)
Thomas Avenue	Gravel	0.621 ± 0.047	0.436 ± 0.021	1.42 ± 0.17	2.16 ± 0.15 (0.59)	2.50 ± 0.13 (0.26)
Ella's Grotto	Sand	0.661 ± 0.078	0.281 ± 0.012	2.36 ± 0.27	5.44 ± 0.56 (1.37)	1.67 ± 0.20 (0.27)
Backslider's Alley	Gravel	0.800 ± 0.055	0.484 ± 0.016	1.65 ± 0.01	2.22 ± 0.12 (0.58)	2.22 ± 0.10 (0.23)
Dyer Avenue	Gravel	0.606 ± 0.041	0.288 ± 0.016	2.10 ± 0.15	4.78 ± 0.31 (1.17)	1.87 ± 0.13 (0.23)
Dismal Valley	Sand	0.108 ± 0.027	0.110 ± 0.010	0.99 ± 0.26	6.51 ± 1.50 (2.32)	3.36 ± 0.42 (0.52)
Collins Avenue	Sand	0.514 ± 0.047	0.308 ± 0.014	1.67 ± 0.15	3.61 ± 0.29 (0.94)	2.28 ± 0.15 (0.26)
Hippodrome	Sand	0.374 ± 0.070	0.389 ± 0.014	0.96 ± 0.18	1.69 ± 0.29 (0.57)	3.20 ± 0.29 (0.40)

*^{26}Al/^{27}Al and ^{10}Be/^{9}Be measured by accelerator mass spectrometry at PRIME Lab. Quartz [Al] measured by flame atomic absorption spectrophotometry and assigned 5% uncertainty. ~0.7 mg ^{9}Be added as carrier to ~100 g quartz samples. ^{10}Be/^{9}Be measured against standards derived from NIST SRM 4325, with an assigned ratio of 3.05×10^{-11}.

†Erosion rates and burial ages inferred from simultaneous solution of equations 1 and 3, assuming local production rates $P_{n,10} = 5.3$ at g^{-1} yr^{-1}, $P_{n,26} = 31.8$ at g^{-1} yr^{-1}, $P\mu,10 = 0.11$ at g^{-1} yr^{-1}, and $P\mu_{,26} = 0.77$ at g^{-1} yr^{-1}. Uncertainties represent one standard error measurement uncertainty, with systematic uncertainties in production rates (20%), production rate ratio, and radioactive decay rates added in quadrature and shown in parentheses.

that are weathered from the limestone. Quartz from each sample (~100 g) was purified by selective chemical dissolution (Kohl and Nishiizumi, 1992), dissolved in HF and HNO_3, and spiked with ~0.7 mg ^{9}Be in a carrier solution prepared from commercial Be metal. After expelling fluorides with H_2SO_4, we separated and purified Al and Be by ion chromatography and then selectively precipitated them as hydroxides. The precipitates were dried, oxidized at 1100 °C, and mixed with Ag powder for accelerator mass spectrometry (AMS) determination of ^{10}Be/^{9}Be and ^{26}Al/^{27}Al at the Purdue Rare Isotope Measurement Laboratory (PRIME Lab). Stable aluminum concentrations in aliquots of the dissolved quartz were determined by flame atomic absorption spectrophotometry (AAS), using the method of standard additions. Little to no matrix effect was observed, and [Al] measurements were reproducible to ~2%. Because [Al] measurements are often difficult to make by AAS, we assigned a generous uncertainty of 5% to all [Al] measurements.

Data Analysis and Uncertainties

Burial dates and preburial erosion rates were determined by iterative solution of equations 1 and 3 (Granger et al., 1997) and are reported in Table 2. Local cosmogenic nuclide production rates are assumed constant, calculated as $P_{10} = 5.4$ at g^{-1} a^{-1} and $P_{26} = 32.6$ at g^{-1} a^{-1} for a latitude of 37° and an elevation of 0.2 km. Production by neutron spallation was scaled using Table 3 of Lal (1991), assuming a sea-level high-latitude ^{10}Be production rate of 4.9 at g^{-1} a^{-1} (Stone et al., 1998) and $P_{26}/P_{10} = 6.0 \pm 0.3$ (from Nishiizumi et al., 1989). Production by muons was scaled for elevation using a local atmospheric pressure of 990 g cm^{-2} (U.S. Standard Atmosphere, 1976) and an atmospheric attenuation length of 240 ± 10 g cm^{-2} (Rossi, 1948), with no latitude dependence (Allkofer and Jokisch, 1973), $P_{26}/P_{10} = 7 \pm 1$ (Heisinger, 1998), and a sea-level ^{10}Be production rate of 0.15 at g^{-1} a^{-1} (Heisinger, 1998). Because the Mammoth Cave region is an area of low relief, production rates do not vary significantly among sediment source areas; a constant production rate is assumed for all samples. A 20% systematic uncertainty assigned to production rates accounts for variations in production rate through time (Frank et al., 1997).

Each result in Table 2 is reported with two separate uncertainties; the first value represents one standard error of analytical uncertainty and is calculated from AMS counting statistics and 5% AAS uncertainty. The second (parenthetical) uncertainty includes systematic uncertainties in radioactive decay rates (8%), P_{26}/P_{10} (5%), absolute production rates (20%), and uncertainty in the ^{10}Be/^{9}Be ratio in the Be spike ($15 \pm 5 \times 10^{-15}$), which must be subtracted from AMS results, with each uncertainty added in quadrature. Analytical uncertainties should be used when comparing burial dates, and total uncertainties should be used when comparing data to calendar ages.

Geological uncertainties, associated with either prior burial or violation of the steady-erosion assumption in equation 1, are defined in two ways. First, gravel collected from the surface (Great Onyx Road; Fig. 2; Tables 2 and 3) shows a burial age of −0.02 ± 0.07 (0.13) Ma, indistinguishable from zero. Second, geological uncertainties are defined by replicate measurements of separate samples collected from either the same site or from separate sites that are clearly related. In the next section, we identify seven geomorphic events in Mammoth Cave's history; for five of these events we use replicate samples to determine geological uncertainties (Table 4). Results of these

comparisons are discussed in a later section on burial dating reproducibility.

Burial dating results are illustrated graphically on a logarithmic plot of $^{26}Al/^{10}Be$ against [^{10}Be] (Fig. 4; after Lal, 1991, modified from Klein et al., 1986). On this diagram, sediments at the surface should plot along the steady erosion curve generated by equation 1, at a position determined by the sample's erosion rate. Upon burial, the $^{26}Al/^{10}Be$ ratio decreases exponentially, in a straight line parallel to the dashed lines of Figure 4. On a logarithmic plot, burial isochrons are distributed linearly, allowing direct visualization of burial dating uncertainty. Note also in Figure 4 that the discrepancy at low [^{10}Be] between the steady erosion and constant exposure curves generated by equations 1 and 2 is due to the importance of muogenic production at quickly eroding sites and the different ^{26}Al and ^{10}Be production-rate ratios due to muons and neutrons.

The steady erosion and constant exposure curves on Figure 4 are nearly linear (Klein et al., 1986), though they appear highly curved on the logarithmic plot. Sediment that is mixed from various sources prior to burial will therefore maintain a $^{26}Al/^{10}Be$ ratio very near these curves, even when [^{26}Al] and [^{10}Be] differ by orders of magnitude among individual clasts (Hancock et al., 1999). Sediment mixing has little effect on burial dating (Granger et al., 1997), though average preburial erosion rates may be underestimated for slow erosion rates where radioactive decay is important (Bierman and Steig, 1996).

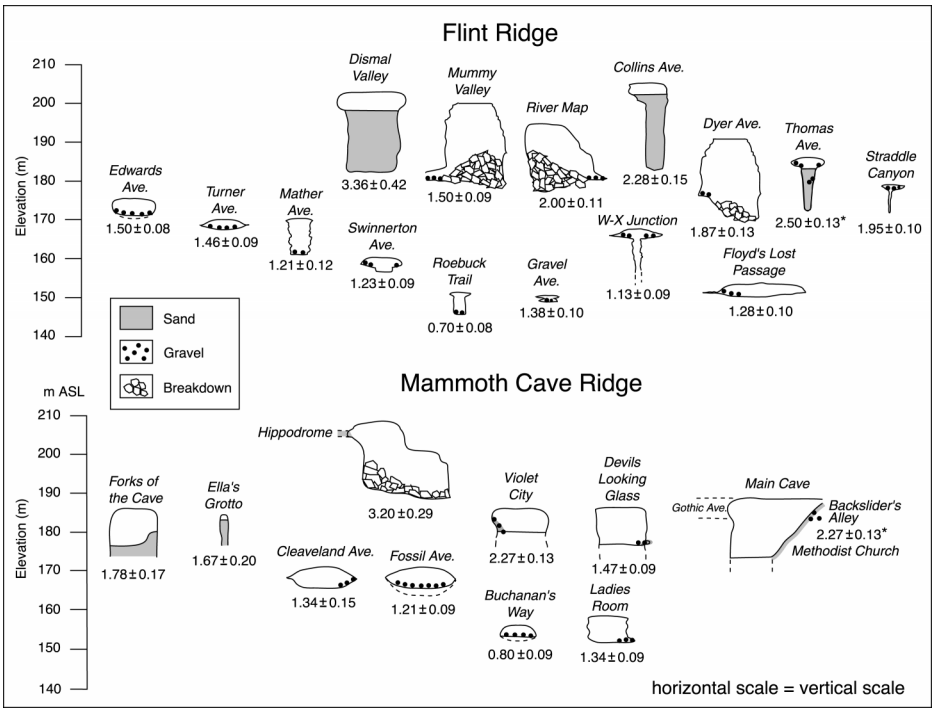

Figure 3. Passage cross sections at sampled locations beneath Flint Ridge and Mammoth Cave Ridge (Fig. 2; Table 3), showing vertical passage relationships and sedimentary fill. Inferred sediment burial ages are shown for each cross section; average ages from multiple samples are denoted by asterisks. ASL—above sea level.

RESULTS AND INTERPRETATION

Mammoth Cave's morphology and sediment stratigraphy permit a sequential reconstruction of water-table position based on previous work by Palmer (1981, 1989) and on our observations here (Table 3). Using the burial dates shown in Table 2 and Figure 4, we identify and date seven events in the cave's development and interpret the history of water-table position as controlled by incision and aggradation of the Green River. Interpretation of each event is based on multiple observations of cave morphology and sediment age, and many are corroborated by surface geomorphology (Table 1). These seven events are illustrated graphically in Figure 5, and are described in detail in the remainder of this section.

1. River Aggradation and Cave Sedimentation at 3.25 ± 0.26 (0.38) Ma

The oldest samples from the cave (Hippodrome and Dismal Valley) were both collected from deep sedimentary fills in vadose canyons at level B far from the Green River (Figs. 2 and 3). Averaging the two ages suggests a period of cave filling ca. 3.25 ± 0.26 (0.38) Ma (all averages are weighted by inverse variance). Prior to sedimentation, the water table must have been lower than the bottom of either passage. Because Dismal Valley is located ~1.5 km upstream from the passage's vadose-phreatic transition, and the canyon slopes 6–9 m/km toward the Green River, we infer that the riverbed was at least 9 m lower than the base of Dismal Valley (i.e., below 174 m) prior to aggradation. Levels A and B must have been formed prior to this date.

2. River Aggradation and Sedimentation of Levels A and B at 2.30 ± 0.20 (0.30) Ma

Passages within Mammoth Cave's level A and level B were all at one time completely filled with sediment (Table 1). We collected seven samples of this passage-filling sediment from four sites distributed throughout the cave. Three samples from Dug Pit in Thomas Avenue have an average age of 2.35 ± 0.25 (0.33) Ma. Two samples from Main Cave (Methodist Church and Backsliders Alley) were collected from within a few meters of each other and have an average age of 2.27 ± 0.30 (0.37) Ma. Sediments were also collected from Violet City (2.27 ± 0.13 [0.25] Ma) and from flood-deposited sediments atop Collins Avenue (2.28 ± 0.15 [0.26] Ma). Assuming that all of these sediments represent a regional sedimentation event, the average age of sediment deposition is 2.30 ± 0.20 (0.30) Ma. Prior to sedimentation, the Green River must have incised to a level below the base of Thomas Avenue, at 173 m. Aggrading cave streams then filled Main Cave with sand and gravel to the ceiling at 188 m, and deposited flood material at the top of Collins Avenue at 203 m. The entire 40 m vertical range of levels A and B has similar sediment dates. Evidence of river aggradation at this time is shown on the surface by broad straths mantled with 10 m of poorly exposed unconsolidated alluvium (Ray, 1996).

3. River Incision From Level B to Level C at 1.92 ± 0.10 (0.21) Ma

Level B and level C passages are separated by narrow vadose canyons and steep tubes, indicating rapid water-table lowering. We define the timing of water-table lowering with two samples: one from level B (Dyer Avenue) indicates that the passage was last active at

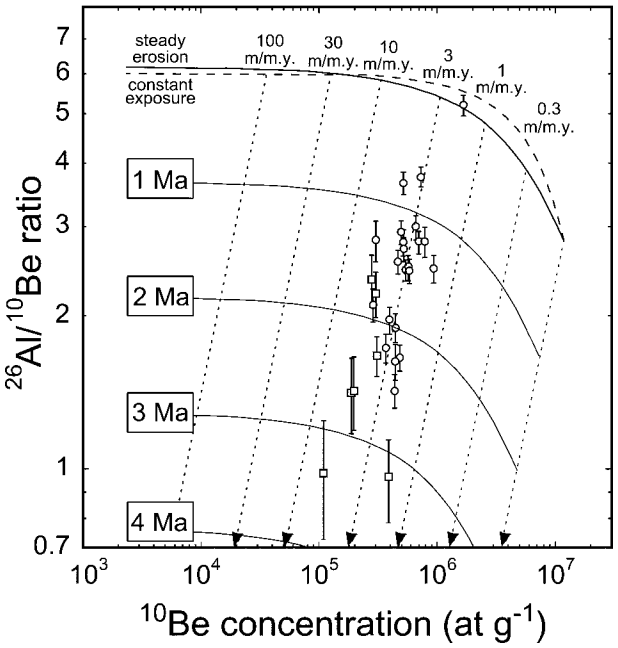

Figure 4. Cosmogenic nuclide data from sediments in the Mammoth Cave system, shown on a logarithmic graph of ^{26}Al/^{10}Be vs. [^{10}Be]. Prior to burial, ^{26}Al/^{10}Be in quartz should fall on the solid steady erosion curve generated by equation 1, at a point determined by the erosion rate of the sediment's source area. Once buried, ^{26}Al/^{10}Be decreases exponentially, parallel to the dashed lines (equation 3). Burial isochrons are shown at million-year intervals; linear spacing facilitates visualization of burial dating uncertainties. Sample burial ages range from 0 Ma (surface sample) to ca. 3.3 Ma, and indicate preburial erosion rates of 1.5–7 m/m.y. (Table 2). The dashed curve (labeled constant exposure) shows ^{26}Al/^{10}Be expected for a sample suddenly exposed to cosmic radiation (equation 2). Circles are gravel samples, and squares are sand samples.

1.87 ± 0.13 (0.23) Ma. A narrow canyon at a slightly lower elevation (Straddle Canyon) shows that the water table was lowering to level C at 1.95 ± 0.10 (0.22) Ma. The average of these two ages implies an episode of rapid Green River incision from level B (186 m) to level C (167 m) at 1.92 ± 0.10 (0.21) Ma. The River Map sample indicates that Salts Cave was an active vadose canyon at this time (2.00 ± 0.11 [0.22] Ma).

4. Local Passage Collapse (Kentucky Avenue) at 1.73 ± 0.15 (0.23) Ma

Kentucky Avenue was a vadose feeder canyon for level B and level C passages before it was blocked by passage collapse. Upon passage collapse, the upstream section and its tributaries filled with ~6 m of sediment, diverting water to a new course through Rose's Pass (Fig. 2). We collected two sand samples from this event, one from the plugged section of Kentucky Avenue (Forks of the Cave), and one from a sediment-filled tributary (Ella's Grotto). The two ages agree very well, 1.78 ± 0.17 (0.25) Ma and 1.67 ± 0.20 (0.27) Ma. The samples were collected ~1 km upstream of the vadose-phreatic transition, indicating that prior to aggradation the river was 6–9 m below the floor at Forks of the Cave, at level C (167 m).

5. River Incision From Level C to Level D at 1.39 ± 0.14 (0.20) Ma

Level C contains wide phreatic tubes with little or no canyon development in their floors, indicating that the passages formed during a long period of river stability followed by rapid incision. Sediments remaining on the floors of level C passages immediately predate passage abandonment and record Green River incision from level C (167 m) to level D (151 m). We collected four gravel samples at this level, including Cleaveland Avenue (1.34 ± 0.15 [0.22] Ma), Fossil Avenue (1.21 ± 0.12 [0.19] Ma), Turner Avenue (1.46 ± 0.09 [0.19] Ma), and Edwards Avenue (1.50 ± 0.08 [0.19] Ma); the average age is 1.39 ± 0.14 (0.20) Ma. A passage at the base of Mummy Valley also dates to roughly this time (1.55 ± 0.09 [0.19] Ma) and was almost certainly an upstream tributary of Edwards Avenue.

6. River Incision Below Level D at 1.24 ± 0.06 (0.16) Ma

Level D passages formed during a period of base-level stability represented on the surface by a strath along the Green River (Miotke and Palmer, 1972). These passages are somewhat smaller than those at level C, suggesting that they formed relatively quickly. We collected gravel from Floyd's Lost Passage (1.28 ± 0.10 [0.18] Ma), Swinnerton Avenue (1.23 ± 0.09 [0.17] Ma), and Mather Avenue (1.21 ± 0.12 [0.19] Ma). The average age of these sediments, 1.24 ± 0.06 (0.16) Ma, is only slightly younger than that of level C passages (event 5), corroborating the geomorphic evidence that water-table stability at this level was short-lived and that the abandonment of level C was achieved by a sudden drop in water table. Two other samples, Gravel Avenue and Ladies Room, are also located at, or just below, level D, but have older sediment dates (Table 2). Because these samples were collected near major passage intersections, it is likely that they contain material transported from upper levels of the cave; we therefore do not include these samples in our estimated age for level D abandonment.

7. River Aggradation ca. 0.7–0.8 Ma

Two samples from complex passages below level D are younger than the rest and indicate an episode of Green River aggradation. Gravel collected from Roebuck Trail (0.70 ± 0.08 [0.15] Ma) and Buchanan's Way (0.80 ± 0.09 [0.16] Ma) were deposited by floodwaters from lower levels. Although Buchanan's Way is slightly higher in the cave than older sediments at level D, scalloped flow marks (Curl, 1974) indicate that floodwaters temporarily bypassed lower levels of the cave through Buchanan's Way to discharge at the Green River (R. Olson, Mammoth Cave National Park, personal commun., 1998).

One sample does not fit neatly into our chronology of cave development. Sediment at Devil's Looking Glass was collected from level B, but dates to 1.47 ± 0.09 (0.19) Ma, far younger than other samples from that level (abandoned at 1.92 ± 0.10 [0.21] Ma; event 3). This sample could indicate either local vadose sedimentation or a brief episode of aggradation that reached the floor of level B.

TABLE 3. SAMPLE DESCRIPTIONS AND INTERPRETATIONS

Sample	Elevation (m)	Cave level	Passage description	Sediment description	Sediment interpretation
Flint Ridge					
Great Onyx Road	Surface			30 cm soil pit with abundant Caseyville gravel	Typical of Caseyville gravel washed into cave
Collins Avenue	203	A	Wide vadose canyon	Cross-bedded sand lens in laminated fine sand and silt	Sandy dikes and rip-up clasts indicate floodwater deposition, probably during sedimentation of level A and B passages
Thomas Avenue	186	B	Vadose canyon filled with 7.6 m sediment to 189 m	Cross-bedded sand and gravel with occasional clay and flowstone	Sedimentation of level A and B passages
Dug Pit Sand	180				
Dug Pit Gravel	180				
Dyer Avenue	186	B	Partially filled vadose canyon	Gravel preserved in wall notch	Deposition by incising stream following sedimentation of level A and B passages; predates level B abandonment.
Dismal Valley	198	B	Wide vadose canyon filled with 15 m sediment to 200 m	Cross-bedded sand	Postdates canyon incision
River Map	180	B	Large vadose canyon	Coarse gravel at base of passage	Postdates Dismal Valley sedimentation
Mummy Valley	180	B	Small vadose passage intersecting base of large vadose canyon filled with 17 m sediment	Coarse gravel in lower passage; canyon is filled with sand and ceiling breakdown	Gravel in lower passage postdates canyon sedimentation
Edwards Avenue	172	C	Phreatic cross section develops into canyon near Green River	Gravel on floor	Immediately predates level C abandonment
Straddle Canyon	178	B–C	Steep vadose tube incised by 2-m-deep, narrow canyon	Gravel in upper tube	Rapid incision between levels B and C
W-X Junction	166	C	Wide but low phreatic tube incised by 15-m-deep, narrow canyon	Gravel in upper tube	Nearby canyons to 30 m deep indicate that passage abandonment occurred long after river incision and water table lowering
Turner Avenue	167	C	Phreatic tube	Gravel on floor	Immediately predates level C abandonment
Mather Avenue	162	C–D	Vadose canyon	Gravel on floor	Dates final occupation of Swinnerton Avenue, downstream; predates level D abandonment
Swinnerton Avenue	158	D	Phreatic tube with shallow vadose trench	Gravel on floor	Immediately predates level D abandonment
Floyd's Lost Passage	151	D	Phreatic tube	Sand and gravel on floor	Immediately predates level D abandonment
Gravel Avenue	149	Below D	Small vadose passage	Gravel on floor	Difficult to interpret; no upstream surface connection implies that sediment may be remobilized from upper levels
Roebuck Trail	146	Below D	Small vadose passage	Calcite-cemented gravels and broken limestone	Within modern flood zone, receives slackwater fines; gravels postdate level D abandonment
Mammoth Cave Ridge					
Hippodrome (Kentucky Avenue)	205	B	Large vadose canyon	Laminated fine sand plugging tributary 2–5 m from top of canyon	Floodwater deposition
Backsliders Alley	186	B	Sediment-filled vadose canyon	Sand and ceiling breakdown with gravel stringers	Sedimentation of levels A and B
Methodist Church	174				
Violet City	180	B	Sediment-filled vadose canyon	Gravel and sand along walls	Sedimentation of levels A and B
Devil's Looking Glass	177	B	Small tributary or alcove alongside partially filled large vadose canyon	Coarse gravel in small tributary to Main Cave	Difficult to interpret; sedimentation of levels A and B (?); alternatively may postdate main passage abandonment
Forks of the Cave (Kentucky Avenue)	177	B	Sediment plug blocking Sandstone Avenue	Cross-bedded sand overlain by laminated muds	Dates passage collapse and diversion of water through Rose's Pass and Boone Avenue
Ella's Grotto	183	B	Sediment filling vadose tributary passage	Cross-bedded sand	Dates passage collapse and diversion of water through Rose's Pass and Boone Avenue
Cleaveland Avenue	166	C	Phreatic tube	Gravel on floor	Immediately predates level C abandonment
Fossil Avenue	167	C	Vadose canyon	Gravel and sand on floor	Immediately predates level C abandonment
Buchanan's Way	152	D	Phreatic tube	Gravel on floor	Difficult to interpret; may represent aggradation and/or floodwater deposition near base level
Ladies Room	152	D	Alcove alongside vadose canyon	Filled with gravel and sand	Difficult to interpret; may represent aggradation and/or floodwater deposition near baselevel

8. Burial Dating Reproducibility

Because we collected multiple samples from clearly related sites throughout the Mammoth Cave system, we can use these data to determine burial dating reproducibility. Replicate samples may not have identical ^{10}Be and ^{26}Al concentrations, which vary with preburial erosion rate and may be specific to individual samples; however, replicate samples should have the same burial age. Five sample suites are clearly related to geomorphic events 2, 3, 4, 5, and 6, and can therefore be used to ascertain reproducibility. Geomorphic evidence for simultaneous deposition is weaker for events 1 and 7, and therefore they are not included in our uncertainty analysis (including them would not alter our conclusions). We

TABLE 4. BURIAL AGE REPRODUCIBILITY

Event	Weighted standard deviation (Ma)	Weighted analytical uncertainty* (Ma)	Reduced χ^2	Probability†
2	0.19 (n = 7)	0.20	1.17	0.32
3	0.06 (n = 2)	0.10	0.24	0.49
4	0.08 (n = 2)	0.15	0.18	0.55
5	0.13 (n = 4)	0.14	1.62	0.18
6	0.04 (n = 3)	0.06	0.12	0.89

*Weighted by inverse variance normalized by average inverse variance following Bevington (1969).
†Probability that analytical uncertainty accounts for all observed variance (should be ~0.5).

also exclude the Devil's Looking Glass sample.

Table 4 shows that in all cases intersample variability is comparable to analytical uncertainty. Reduced χ^2 values near 1.0 show that analytical uncertainty can account for all of the observed intersample variability. Nonetheless, close examination of the data reveals systematic differences between gravel and sand samples. For example, in three samples from Dug Pit in Thomas Avenue, sand yielded a burial age of 2.65 ± 0.28 (0.37) Ma and two gravel samples yielded ages of 2.19 ± 0.11 (0.24) Ma and 2.50 ± 0.13 (0.26) Ma. The age inferred from sand is slightly older than the gravel ages, although indistinguishable at two standard errors. Likewise, sand from Methodist Church yielded a burial age of 2.62 ± 0.27 (0.36) Ma while gravel from the same deposit at Backsliders Alley yielded a younger age of 2.22 ± 0.10 (0.23) Ma, although the difference is indistinguishable at two standard errors. It is possible that some sand enters the cave with a burial signal inherited from time spent buried in doline floors, or that floods remobilize sand from upper levels of the cave.

In addition, sand and gravel samples show a systematic difference in their inherited cosmogenic nuclide concentrations. In general, sand represents a slightly faster erosion rate than gravel (5–7 m/m.y. for sand vs. 1.5–6 m/m.y. for gravel). Statistical differences in erosion rate may be confounded by samples being derived from different catchments eroding at different rates, variations in erosion rate through time, and variations in cosmogenic nuclide production rates through time. Nonetheless, average erosion rates inferred from gravel (2.89 ± 0.21 m/m.y. [n = 21]) and sand (3.96 ± 0.61 m/m.y. [n = 7]) are distinguishable with 90% statistical confidence. Contrasting erosion rates of the Big Clifty sandstone and the Caseyville conglomerate are also reflected in the landscape, where the erosion-resistant conglomerate forms knobs and ridges that protrude above surrounding sandstone.

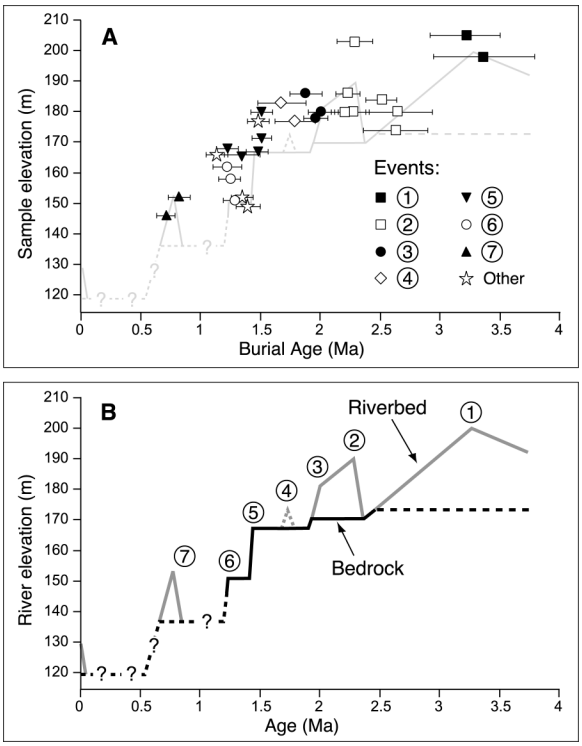

Figure 5. Green River history inferred from Mammoth Cave burial ages. Circled numbers refer to seven key events discussed in text. (A) Cave sediment burial ages plotted against elevation. Error bars represent one standard error analytical uncertainty. Note that the seven key events are clearly distinguishable, and that ages inferred for each event overlap within uncertainty. Faint lines show lines of B. Stars represent data not included in our interpretation (see text and Table 3 for details). (B) Riverbed and bedrock elevations are inferred from cave-passage morphology, sedimentology, and sediment burial ages. River aggradation is indicated by divergence of the riverbed (gray line) and bedrock (black line). Dashed bedrock line indicates maximum bedrock elevation where uncertain. Note increased bedrock incision rate ca. 1.5 Ma, from 3–5 m/m.y. to >30 m/m.y., associated with creation of the Ohio River.

DISCUSSION

Dating the water-table history at Mammoth Cave has regional significance. Cave levels were controlled by development of the Green River valley, which in turn was influenced by the Ohio River. The geomorphic evolution of the Ohio River and its tributaries, and hence Mammoth Cave, is intimately linked to the history of Pliocene−Pleistocene glaciation (Miotke and Palmer, 1972; Melhorn and Kempton, 1991; Granger and Smith, 2000). In the next section we propose correlations that relate our inferred incision and aggradation events on the Green River with important climatic changes and drainage rearrangements in the eastern United States. We then compare our data with previous work at Mammoth Cave and discuss some of the implications of our results for landscape evolution in the Interior Low Plateaus.

River Incision and Climate History

Climate during middle Pliocene time in Kentucky was probably comparable to, or slightly warmer than, that of the present (cf. Groot, 1991). Mammoth Cave's morphology together with our sediment dates indicate that the Green River at that time was incising very slowly, promoting dissolution of the very large passages of level A and level B. River incision rates into bedrock in late Pliocene time were <3–5 m/m.y. (Fig. 5). The Green River eroded a wide valley at 175–180 m elevation in the Mammoth Cave area, remnants of which are preserved as prominent strath terraces (Ray, 1996). Vast areas of exposed limestone were denuded to near river level on the

Pennyroyal surface southeast of the Green River (Fig. 2).

At 3.25 ± 0.26 (0.38) Ma, the Green River aggraded with sediment, filling Mammoth Cave (event 1). The cause of river aggradation is uncertain, but marine oxygen isotope records reveal that general climatic cooling and ice-sheet growth began at that time. The Green River slowly excavated its valley fill over the next ~0.9 m.y. and incised a few meters into bedrock, partly emptying Mammoth Cave of its sediments and promoting vadose canyon incision. At 2.30 ± 0.20 (0.30) Ma, the river once again aggraded, filling Mammoth Cave with 15–20 m of sediment (event 2). This prominent aggradation event probably correlates with the appearance of the first large Northern Hemisphere ice sheets ca. 2.4 Ma. Oxygen isotope records from the Gulf of Mexico reveal that an ice sheet advanced into the Mississippi River drainage at that time (Joyce et al., 1993, modified to the time scale of Shackleton et al., 1990). Although the ice did not reach the latitude of the Green River, climate in the area would have been cooler and drier during the glacial maximum. Potential causes of river aggradation may have been increased erosion rates in the uplands due to changing vegetation, a stormier climate, or reduced river discharge.

The Green River subsequently incised through its accumulated sediments, reaching the lower part of level B (186 m) after 0.3–0.4 m.y.. At 1.92 ± 0.10 (0.21) Ma (event 3), the Green River quickly cut through the remaining sediments in its valley and incised into bedrock for a few meters, stabilizing at level C (167 m). This incision event may correlate with a major ice advance ca. 2 Ma. Ice sheets at this time advanced into Iowa and Nebraska, as shown by magnetically reversed glacial sediments beneath a volcanic ash dated at 2.01 Ma (Boellstorff, 1978); these tills have been correlated to the Réunion paleomagnetic excursion at 2.14 Ma (Hallberg, 1986). Oxygen isotope excursions in the Gulf of Mexico also record a prominent glacial meltwater spike ca. 2 Ma (Joyce et al., 1993, modified to the time scale of Shackleton et al., 1990). Sedimentation rates on the Mississippi fan increased at this time, consistent with extensive glaciation in the watershed. It is possible that the Teays River formed along the glacial margin at this time at the latitude of central Indiana and Ohio (Fig. 1; Gray, 1991). Although ice lobes reached far south, they did not reach the preglacial Old Ohio River and therefore only indirectly affected the Green River.

The Green River remained near the elevation of level C for ~0.5 m.y., until it suddenly incised through 15 m of bedrock at 1.39 ± 0.14 (0.20) Ma (event 5) and stabilized again at level D (151 m). This incision event probably correlates with the formation of the Ohio River along an ice-sheet margin. Several lines of evidence support formation of the Ohio River at this time. Granger and Smith (2000) used $^{26}Al/^{10}Be$ methods to date proglacial sediments that were deposited when the preglacial old Kentucky River was dammed and diverted westward to join the Old Ohio River, defining the course of the modern Ohio River across this preglacial divide (Ray, 1974). Sediments within an abandoned stretch of the old Kentucky River date to 1.5 ± 0.3 Ma. Moreover, sedimentation rates on the Mississippi fan dramatically increased at 1.4–1.5 Ma (Pulham, 1993; Villamil et al., 1998), consistent with extensive glaciation within the Mississippi watershed and formation of the present course of the Ohio River at that time.

Once the Ohio River established its present course, it quickly incised and became a major sluiceway for glacial meltwater and outwash valley trains. The Green River, as a tributary of the Ohio River, underwent frequent changes in base level as the Ohio alternately filled and incised with the fluctuating ice sheets. The marine isotope record reveals that the next large ice sheet postdating formation of the Ohio River occurred ca. 1.2 Ma. This ice sheet may have crossed the Ohio River locally, depositing till on a bench ~30 m below the course of the Old Ohio River (Ray, 1974). It is possible that this ice sheet correlates with Green River incision at 1.24 ± 0.06 (0.16) Ma (event 6) that caused abandonment of Mammoth Cave's level D and marked the end of river stability and development of clearly defined cave levels (Miotke and Palmer, 1972; Palmer, 1989, 1991).

The final event we infer from Mammoth Cave sediments is river aggradation ca. 0.7–0.8 Ma (event 7). This sedimentation correlates with very large marine isotope excursions at stages 20 and 22, and may represent aggradation behind a valley train in the Ohio River. Sedimentation rates on the Mississippi fan again increased at 0.7–0.8 Ma, consistent with extensive glaciation and valley trains at that time. At present, the Green River valley at Mammoth Cave is filled with 10 m of sediment that accumulated behind Wisconsinan valley trains in the Ohio River (Miotke and Palmer, 1972). The lowermost cave passages are flooded and many are filled with sediment. They are a modern analog for the cave's response to river aggradation.

Comparison With Earlier Work

Earlier dating at Mammoth Cave showed the antiquity of the cave but was unable to assign a precise chronology to river incision and cave development. Schmidt (1982) estimated a water table lowering rate using the magnetic polarity of fine-grained sediments in the cave. The lowermost magnetically reversed samples were found at level C (167 m), showing that these passages were in the flood zone prior to the Brunhes-Matuyama transition at 0.78 Ma (Cande and Kent, 1995). Modern floods deposit fine-grained sediment more than 20 m above river base level, so the Green River could have been well below these passages when the sediment was deposited. Our coarse-grained samples show that the water table dropped below level C at 1.39 ± 0.14 (0.20) Ma (event 5), and are consistent with Schmidt's results. Paleomagnetic data from higher in the cave system are more difficult to correlate with specific reversals; Schmidt assumed a constant river incision rate and calculated that the uppermost cave passages would be younger than 2 Ma. Our cosmogenic data and the cave's morphology suggest that river incision was episodic and more rapid in the Pleistocene, and are inconsistent with Schmidt's proposed ages. Schmidt's paleomagnetic data, however, are compatible with ours, keeping in mind that floodwaters at 2 Ma could have reached the cave's uppermost passages.

The only other radiometric geochronology done at Mammoth Cave was by Hess and Harmon (1981), who used U-Th ratios to show that flowstone at level D is older than 0.35 Ma. This is consistent with our cosmogenic results, which show that the passage was last occupied by sediment-transporting streams ca. 0.7 Ma.

Implications for Landscape Evolution

The erosion rate determined for sandstone- and conglomerate-capped ridges in the Mammoth Cave region (1.72 ± 0.07 [0.39] m/m.y.; Table 2) is among the slowest reported for North America. Bierman et al. (1995) and Bierman and Turner (1995) reported comparable rates for granitic inselbergs in the Alabama Hills, California (1.6 m/m.y.), the Llano uplift, Texas (2.4 m/m.y.), and northern Georgia (2–10 m/m.y.). Pavich et al. (1985) reported a bedrock-lowering rate of 4.5–8 m/m.y. in the Virginia piedmont. These erosion rates are comparable to those from other stable continental interiors such as West Africa (3–8 m/m.y.; Brown et al., 1992), southern Africa

(5 m/m.y.; Cockburn et al., 1999), Venezuela (~1 m/m.y.; Brown et al., 1992), and Australia (0.6–1 m/m.y.; Bierman and Turner, 1995). Such slow erosion rates may be the norm in unglaciated and tectonically stable continental interiors. Slower erosion rates have been found only in extremely arid environments, such as polar deserts (<0.1–1 m/m.y.; Nishiizumi et al., 1991).

Measurements of ^{26}Al and ^{10}Be in Mammoth Cave's sediments indicate that ridgetop erosion rates have remained virtually unchanged over the past 3–4 m.y., despite accelerated river incision at a rate of ~30 m/m.y. (Fig. 5). River incision has outpaced hillslope erosion for more than 2 m.y., resulting in river entrenchment within a steep-walled valley. We infer that river entrenchment is primarily a result of drainage rearrangement to the north, especially integration of the Teays River system ca. 2 Ma and integration of the Ohio River system ca. 1.5 Ma. These ice-marginal rivers, having larger drainage areas and a shorter path to the sea than their predecessors, rapidly incised through previously undissected uplands and initiated episodes of rapid incision throughout the drainage network.

CONCLUSIONS

The sediment chronology determined from cosmogenic ^{26}Al and ^{10}Be shows that Mammoth Cave's evolution, and, by extension, the incision history of the Green River, occurred in step with major climate changes and drainage reorganizations. Sedimentation of the upper levels of the Mammoth Cave system occurred simultaneously with the growth of the first large ice sheets in North America in late Pliocene time (e.g., Raymo, 1994). Successively larger ice sheets extended southward in late Pliocene and early Pleistocene time, damming rivers and permanently diverting drainage patterns along ice margins in the Interior Low Plateaus region. Drainage systems were reorganized and incised into bedrock at least twice, as ice first advanced to the latitude of central Indiana and Ohio to form the Teays River and later advanced farther south to form the Ohio River (Gray, 1991). River incision and canyon entrenchment in the Interior Low Plateaus region is primarily due to rapid downcutting of these newly formed rivers. The data from Mammoth Cave suggest that incision due to integration of the Teays River network occurred near 2 Ma, and that rapid incision associated with diversion of the Ohio River occurred near 1.5 Ma. This timing is consistent with sedimentation and meltwater spikes in the Gulf of Mexico (Pulham, 1993; Joyce et al., 1993), till stratigraphy (Ray, 1974; Boellstorff, 1978), and the reversed magnetic polarity of proglacial lake clays (Bonnett et al., 1991).

Later glaciations are represented at Mammoth Cave by river incision ca. 1.2–1.3 Ma, and by aggradation at 0.7–0.8 Ma. These two glaciations are consistent with till stratigraphy along the Ohio River (Ray, 1974), glacial diversion of the Ohio River at Cincinnati, Ohio (Durrell, 1961), and marine oxygen isotope records (e.g., Raymo, 1994).

The data from Mammoth Cave also have significant implications for landscape evolution in the Interior Low Plateaus. Sandstone- and conglomerate-capped uplands are eroding very slowly, and have been since at least middle Pliocene time, despite accelerated river incision rates. The lack of an integrated surface drainage in the Mammoth Cave area undoubtedly decouples hillslope erosion and river incision to some degree. However, the presence of steep-walled valleys throughout the Interior Low Plateaus suggests that hillslope erosion significantly lags accelerated river incision rates across the entire region.

This work does not resolve several important issues in landscape evolution of the Mammoth Cave area, e.g., (1) the rate at which hillslopes respond to accelerated river incision; (2) whether river incision occurred as knickpoints propagating upriver or as more gradual steepening; and (3) the reason the most extensive ice lobe in the Interior Low Plateaus occurred so early, when marine isotope records suggest global ice volumes significantly less than those in late Pleistocene time. Resolving these issues will require additional river incision studies, as well as dating the many enigmatic pre-Illinoian glacial deposits in the eastern United States.

ACKNOWLEDGMENTS

We are grateful to Joe Meiman, hydrologist at Mammoth Cave National Park, for his help organizing this project, and to Mammoth Cave National Park for permission to work and collect sediment samples in the park. Many members of the Cave Research Foundation assisted us in the caves. We appreciate assistance from, and discussions with, Darlene Anthony, Phil Bodanza, Don Coons, Chris Groves, Jason Gulley, Jarda Kadlec, Rick Olson, Peg Palmer, Joe Ray, Rickard Toomey, and Richard Zopf. Allison Granger assisted in sample preparation. This research was funded by National Science Foundation grant EAR-9706011.

REFERENCES CITED

Allkofer, O.C., and Jokisch, H., 1973, A survey of the recent measurements of the absolute vertical cosmic-ray muon flux at sea level: Il Nuovo Cimento, v. 15A, p. 371–389.

Bierman, P.R., and Steig, E.J., 1996, Estimating rates of denudation using cosmogenic isotope abundances in sediment: Earth Surface Processes and Landforms, v. 21, p. 125–139.

Bierman, P., and Turner, J., 1995, ^{10}Be and ^{26}Al evidence for exceptionally low rates of Australian bedrock erosion and the likely existence of pre-Pleistocene landscapes: Quaternary Research, v. 44, p. 378–382.

Bierman, P., Gillespie, A., Caffee, M., and Elmore, D., 1995, Estimating erosion rates and exposure ages with ^{36}Cl produced by neutron activation: Geochimica et Cosmochimica Acta, v. 59, p. 3779–3798.

Bierman, P.R., Marsella, K.A., Patterson, C., Davis, P.T., and Caffee, M., 1999, Mid-Pleistocene cosmogenic minimum-age limits for pre-Wisconsinan glacial surfaces in southwestern Minnesota and southern Baffin Island: A multiple nuclide approach: Geomorphology, v. 27, p. 25–39.

Bilokon, H., Castagnoli, G.C., Castellina, A., Piazzoli, B.D.E., Mannocchi, G., Meroni, E., Picchi, P., and Vernetto, S., 1989, Flux of the vertical negative muons stopping at depths 0.35–1000 hg/cm^2: Journal of Geophysical Research, v. 94, no. B9, p. 12145–12152.

Bocchini, A., and Coltorti, M., 1990, Il complesso carsico Grotta del Fiume-Grotta Grande del Vento e l'evoluzione geomorfologica della Gola di Frassassi, *in* Galdenzi, S., and Menechetti, M., eds., Il carsismo della Gola di Frasassi, Memori Instituto Italiano de Speleologia, v. 4, p. 155–180.

Boellstorff, J., 1978, A need for redefinition of North American Pleistocene stages: Gulf Coast Association of Geological Societies Transactions, v. 28, p. 65–74.

Bonnett, R.B., Noltimier, H.C., and Sanderson, D.D., 1991, A paleomagnetic study of the early Pleistocene Minford Silt Member, Teays Formation, West Virginia, *in* Melhorn, W.N., and Kempton, J.P., eds., Geology and hydrogeology of the Teays-Mahomet bedrock valley system: Geological Society of America Special Paper 258, p. 9–18.

Brown, E.T., Stallard, R.F., Raisbeck, G.M., and Yiou, F., 1992, Determination of the denudation rate of Mount Roraima, Venezuela using cosmogenic ^{10}Be and ^{26}Al: Eos (Transactions, American Geophysical Union), v. 73, p. 170.

Brown, E.T., Bourles, D.L., Colin, F., Sanfo, Z., Raisbeck, G.M., and Yiou, F., 1994, The development of iron crust lateritic systems in Burkina Faso, West Africa, examined with in-situ−produced cosmogenic nuclides: Earth and Planetary Science Letters, v. 124, p. 19–33.

Brown, E.T., Stallard, R.F., Larsen, M.C., Raisbeck, G.M., and Yiou, F., 1995, Denudation rates determined from the accumulation of in situ-produced ^{10}Be in the Luquillo Experimental Forest, Puerto Rico: Earth and Planetary Science Letters, v. 129, p. 193–202.

Cande, S.C., and Kent, D.V., 1995, Revised calibration of the geomagnetic polarity time scale for the Late Cretaceous and Cenozoic: Journal of Geophysical Research, v. 100, no. B4, p. 6093–6095.

Cockburn, H.A.P., Seidl, M.A., and Summerfield, M.A., 1999, Quantifying denudation rates on inselbergs in the central Namib Desert using in situ-produced cosmogenic ^{10}Be and ^{26}Al: Geology, v. 27, p. 399–402.

Curl, R.L., 1974, Deducing flow velocity in cave conduits from scallops: National Speleological Society Bulletin, v. 36, p. 1–5.

Davies, W.E., 1960, Origin of caves in folded limestone: National Speleological Society Bulletin, v. 22, p. 5–18.

Davies, W.E., and LeGrand, H.E., 1972, Karst of the United States, *in* Herak, M., and Stringfield, V.T., eds., Karst: Important karst regions of the Northern Hemisphere: Amsterdam, Elsevier, p. 467–505.

Dreybrodt, W., 1996, Principles of early development of karst conduits under natural and man-made conditions revealed by mathematical analysis of numerical models: Water Resources Research, v. 32, p. 2923–2935.

Durrell, R.H., 1961, The Pleistocene geology of the Cincinnati area, Field Trip 3 *in* Guidebook for field trips,

Geological Society of America Annual Meeting: Cincinnati, Ohio, University of Cincinnati, p. 47–64.
Fabel, D., and Harbor, J., 1999, Applications of in situ cosmogenic radionuclide techniques in glaciology and glacial geomorphology: Annals of Glaciology, v. 28, p. 103–110.
Fenneman, N.M., 1938, Physiography of the eastern United States: New York, McGraw-Hill, 714 p.
Fisk, H.N., 1944, Geological investigation of the alluvial valley of the lower Mississippi River: Vicksburg, Mississippi, U.S. Army Corps of Engineers, Mississippi River Commission, 78 p.
Ford, D.C., and Williams, P.W., 1989, Karst geomorphology and hydrology: London, Chapman and Hall, 601 p.
Frank, M., Schwartz, B., Baumann, S., Kubik, P.W., Suter, M., and Mangini, A., 1997, A 200 kyr record of cosmogenic radionuclide production from ^{10}Be in globally stacked deep-sea sediments: Earth and Planetary Science Letters, v. 149, p. 121–129.
Granger, D.E., Kirchner, J.W., and Finkel, R., 1996, Spatially averaged long-term erosion rates from in-situ produced cosmogenic nuclides in alluvial sediment: Journal of Geology, v. 104, p. 249–257.
Granger, D.E., Kirchner, J.W., and Finkel, R.C., 1997, Quaternary downcutting rate of the New River, Virginia, measured from differential decay of cosmogenic ^{26}Al and ^{10}Be in cave-deposited alluvium: Geology, v. 25, p. 107–110.
Granger, D.E., and Smith, A.L., 2000, Dating buried sediments using radioactive decay and muogenic production of ^{26}Al and ^{10}Be: Nuclear Instruments and Methods in Physics Research B, v. 172, p. 822–826.
Gray, H.H., 1991, Origin and history of the Teays drainage system; the view from midstream, *in* Melhorn, W.N., and Kempton, J.P., eds., Geology and hydrogeology of the Teays-Mahomet bedrock valley system: Geological Society of America Special Paper 258, p. 43–50.
Groot, J.J., 1991, Palynological evidence for late Miocene, Pliocene, and Pleistocene climate changes in the middle U.S. Atlantic coastal plain: Quaternary Science Reviews, v. 10, p. 147–162.
Hallberg, G.R., 1986, Pre-Wisconsin glacial stratigraphy of the central plains region in Iowa, Nebraska, Kansas and Missouri: Quaternary Science Reviews, v. 5, p. 11–15.
Hancock, G.S., Anderson, R.S., Chadwick, O.A., Finkel, R.C., 1999, Dating fluvial terraces with ^{10}Be and ^{26}Al profiles: Application to the Wind River, Wyoming Geomorphology, v. 27, p. 41–60.
Heimsath, A.M., Dietrich, W.E., Nishiizumi, K., and Finkel, R.C., 1997, The soil production function and landscape equilibrium: Nature, v. 388, p. 358–361.
Heisinger, B.P., 1998, Myonen-induzierte produktion von radionukliden [Ph.D. thesis]: Munich, Technischen Universität München, 153 p.
Heisinger, B., Niedermayer, M., Hartmann, F.J., Korschinek, G., Nolte, E., Morteani, G., Neumaier, S., Petitjean, C., Kubik, P., Synal, A., and Ivy-Ochs, S., 1997, In situ production of radionuclides at great depths: Nuclear Instruments and Methods in Physics Research B, v. 123, p. 341–346.
Hess, J.W., and Harmon, R.S., 1981, Geochronology of speleothems from the Flint Ridge Mammoth Cave system, Kentucky, USA: Proceedings of the International Congress on Speleology, v. 8, p. 433–436.
Hofmann, H.J., Beer, J., Bonani, G., Von Gunten, H.R., Raman, S., Suter, M., Walker, R.L., Wolfli, W., and Zimmerman, D., 1987, ^{10}Be: Half-life and AMS-standards: Nuclear Instruments and Methods in Physics Research, v. B29, p. 32–36.
Iribane, J.V., and Godson, W.L., 1992, Atmospheric thermodynamics: Dordrecht, D. Reidel, 259 p.
Joyce, J.E., Tjalsma, L.R.C., and Prutzman, J.M., 1993, North American glacial meltwater history for the past 2.3 m.y.: Oxygen isotope evidence from the Gulf of Mexico: Geology, v. 21, p. 483–486.
Klein, J., Giegengack, R., Middleton, R., Sharma, P., Underwood, J.R.J., and Weeks, R.A., 1986, Revealing histories of exposure using in situ produced ^{26}Al and ^{10}Be in Libyan desert glass: Radiocarbon, v. 28, no. 2A, p. 547–555.
Kohl, C.P., and Nishiizumi, K., 1992, Chemical isolation of quartz for measurement of in-situ−produced cosmogenic nuclides: Geochimica et Cosmochimica Acta, v. 56, p. 3583–3587.
Kubik, P.W., Ivy-Ochs, S., Masarik, J., Frank, M., and Schlüchter, C., 1998, ^{10}Be and ^{26}Al production rates deduced from an instantaneous event within the dendro-calibration curve, the landslide of Köfels, Ötz valley, Austria: Earth and Planetary Science Letters, v. 161, p. 231–241.
Lal, D., 1991, Cosmic ray labeling of erosion surfaces: In situ nuclide production rates and erosion models: Earth and Planetary Science Letters, v. 104, p. 424–439.
Lal, D., and Arnold, J.R., 1985, Tracing quartz through the environment: Indian Academy of Science Proceedings, Earth and Planetary Science, v. 94, p. 1–5.
Lal, D., and Peters, B., 1967, Cosmic ray produced radioactivity on the Earth, *in* Flugge, S., ed., Handbuch der Physik: Berlin, Springer-Verlag, p. 551–612.
Masarik, J., and Reedy, R.C., 1995, Terrestrial cosmogenic-nuclide production systematics calculated from numerical simulations: Earth and Planetary Science Letters, v. 136, p. 381–395.
Melhorn, W.N., and Kempton, J.P., eds., 1991, Geology and hydrogeology of the Teays-Mahomet bedrock valley system: Geological Society of America Special Paper 258, 128 p.
Middleton, R., and Klein, J., 1987, ^{26}Al: measurement and applications: Royal Society of London Philosophical Transactions, ser. A., v. 323, p. 121–143.
Miotke, F.-D., and Palmer, A.N., 1972, Genetic relationship between caves and landforms in the Mammoth Cave National Park area: Würtzburg, Germany, Böhler Verlag, 69 p.
Nishiizumi, K., Winterer, E.L., Kohl, C.P., Klein, J., Middleton, R., Lal, D., and Arnold, J.R., 1989, Cosmic ray production rates of ^{10}Be and ^{26}Al in quartz from glacially polished rocks: Journal of Geophysical Research, v. 94, no. B12, p. 17907–17915.
Nishiizumi, K., Kohl, C.P., Arnold, J.R., Klein, J., Fink, D., and Middleton, R., 1991, Cosmic ray produced ^{10}Be and ^{26}Al in Antarctic rocks: Exposure and erosion history: Earth and Planetary Science Letters, v. 104, p. 450–454.
Norris, T.L., Gancarz, A.J., Rokop, D.J., and Thomas, K.W., 1983, Half-life of ^{26}Al: Proceedings of the Fourteenth Lunar and Planetary Science Conference, Part I: Journal of Geophysical Research, v. 88, p. B331–B333.
Palmer, A.N., 1977, Influence of geologic structure on groundwater flow and cave development in Mammoth Cave National Park, Kentucky, USA, *in* Tolson, J.S., and Doyel, F.L., eds., Karst hydrogeology, International Association of Hydrogeologists Memoir 12, p. 405–414.
Palmer, A.N., 1981, A geological guide to Mammoth Cave National Park: Teaneck, New Jersey, Zephyrus Press, 196 p.
Palmer, A.N., 1989, Geomorphic history of the Mammoth Cave system, *in* White, W.B., and White, E.L., eds., Karst hydrogeology: Concepts from the Mammoth Cave area: New York, Van Nostrand Reinhold, p. 317–337.
Palmer, A.N., 1991, Origin and morphology of limestone caves: Geological Society of America Bulletin, v. 103, p. 1–21.
Pavich, M.J., Brown, L., Valette-Silver, J.N., Klein, J., and Middleton, R., 1985, ^{10}Be analysis of a Quaternary weathering profile in the Virginia Piedmont: Geology, v. 13, p. 39–41.
Potter, P.E., 1955, The petrology and origin of the Lafayette gravel, Part 2. Geomorphic history: Journal of Geology, v. 63, p. 115–132.
Powell, R.L., 1970, Base level, lithologic, and climatic controls of karst groundwater zones in south-central Indiana: Indiana Academy of Sciences Proceedings, v. 79, p. 281–291.
Pulham, A.J., 1993, Variations in slope deposition, Pliocene-Pleistocene, offshore Louisiana, northeast Gulf of Mexico, *in* Weimer, P., and Posamentier, H., eds., Siliciclastic sequence stratigraphy: Recent developments and applications: American Association of Petroleum Geologists Memoir 58, p. 199–233.
Ray, J.A., 1996, Fluvial features of the karst-plain erosion surface in the Mammoth Cave region, 5th Mammoth Cave National Park Science Conference, Mammoth Cave, Kentucky: Mammoth Cave, Kentucky, National Park Service, p. 137–156.
Ray, L.L., 1974, Geomorphology and Quaternary geology of the glaciated Ohio River Valley—A reconnaissance study: U.S. Geological Survey Professional Paper 826, 77 p.
Raymo, M.E., 1994, The initiation of Northern Hemisphere glaciation: Annual Review of Earth and Planetary Sciences, v. 22, p. 353–383.
Repka, J.L., Anderson, R.S., and Finkel, R.C., 1997, Cosmogenic dating of fluvial terraces, Fremont River, Utah: Earth and Planetary Science Letters, v. 152, p. 59–73.
Rossi, B., 1948, Interpretation of cosmic-ray phenomena: Reviews of Modern Physics, v. 20, p. 537–583.
Royall, P.D., Delcourt, P.A., and Delcourt, H.R., 1991, Late Quaternary paleoecology and paleoenvironments of the central Mississippi alluvial valley: Geological Society of America Bulletin, v. 103, p. 157–170.
Schmidt, V.A., 1982, Magnetostratigraphy of sediments in Mammoth Cave, Kentucky: Science, v. 217, p. 827–829.
Shackleton, N.J., Berger, A., and Peltier, W.R., 1990, An alternative astronomical calibration of the lower Pleistocene time scale based on ODP site 677: Royal Society of Edinburgh Transactions, Earth Sciences, v. 81, p. 251–161.
Small, E.E., Anderson, R.S., and Hancock, G.S., 1999, Estimates of the rate of regolith production using ^{10}Be and ^{26}Al from an alpine hillslope: Geomorphology, v. 27, p. 131–150.
Stone, J.O.H., Evans, J.M., Fifield, L.K., Allan, G.L., and Cresswell, R.G., 1998, Cosmogenic chlorine-36 production in calcite by muons: Geochimica et Cosmochimica Acta, v. 62, p. 433–454.
Teller, J.T., and Goldthwait, R.P., 1991, The old Kentucky River; a major tributary to the Teays River, *in* Melhorn, W.N., and Kempton, J.P., eds., Geology and hydrogeology of the Teays-Mahomet bedrock valley system: Geological Society of America Special Paper 258, p. 29–41.
Thornbury, W.D., 1965, Regional geomorphology of the United States: New York, John Wiley & Sons, Inc, 609 p.
Tight, W.G., 1903, Drainage modifications in southeastern Ohio and adjacent parts of West Virginia and Kentucky: U.S. Geological Survey Professional Paper 13, 111 p.
Villamil, T., Arango, C., Weimer, P., Waterman, A., Rowan, M.G., Varnai, P., Pulham, A.J., and Crews, J.R., 1998, Biostratigraphic techniques for analyzing benthic biofacies, stratigraphic condensation, and key surface identification, Pliocene and Pleistocene sediments, northern Green Canyon and Ewing Bank (Offshore Louisiana), northern Gulf of Mexico: American Association of Petroleum Geologists Bulletin, v. 82, p. 961–985.
White, E.L., and White, W.B., 1968, Dynamics of sediment transport in limestone caves: National Speleological Society Bulletin, v. 30, p. 115–129.
White, W.B., 1988, Geomorphology and hydrology of karst terrains: New York, Oxford University Press, 464 p.

MANUSCRIPT RECEIVED BY THE SOCIETY APRIL 24, 2000
REVISED MANUSCRIPT RECEIVED JULY 5, 2000
MANUSCRIPT ACCEPTED AUGUST 21, 2000

Printed in the USA